Joining by forming technology for thermal applications: A case study of finned tube heat exchanger

Supplementary Material for Joining by forming technology for thermal applications: A case study of finned tube heat exchanger

Riccardo Saltarelli[1], Luís M. Alves[2], Matteo Fasano[(1)] and Rafael M. Afonso [(2*)]*

[1]Dipartimento Energia, Politecnico di Torino, Corso Duca degli Abruzzi 24, 10129 Torino, Italy

[2]IDMEC, Instituto Superior Técnico, University of Lisbon, Av. Rovisco Pais, 1049-001 Lisbon, Portugal

(*) rafael.afonso@tecnico.ulisboa.pt, matteo.fasano@polito.it

SUPPLEMENTARY NOTE 1

The fluid dynamics was simulated considering the following assumptions: steady-state three-dimensional flow; homogeneous, Newtonian, and incompressible fluids; negligible radiative heat transfer and viscous heating; no-slip conditions; gravity and entrance effects neglected [1]. The turbulence model chosen was a realizable $k-\varepsilon$ (being k the turbulent kinetic energy and ε the rate of dissipation of turbulent kinetic energy) [2], with enabled energy equation and enhanced wall treatment option. Enabling the energy equation on ANSYS Fluent® means allowing the user to set energy or heat transfer related parameters in the simulation [3]. The realizable $k-\varepsilon$ model differs from the standard model in two aspects: first, the realizable model contains an alternative formulation for the turbulent viscosity μ_t and second, a modified transport equation for ε is used. The adjective "realizable" highlights how the model satisfies some mathematical constraints on the Reynolds stresses, coherently with the physics of turbulent flows.

Given these assumptions, the governing RANS equations ($u_i = \overline{u_i} + u_i'$, being u_i the velocity in the i direction, $\overline{u_i}$ its mean and u_i' fluctuating components) adopted in the CFD model were the following:

- Continuity equation

$$\frac{\partial}{\partial x_i}(\rho \overline{u_i}) = 0, \tag{S1}$$

being ρ the fluid density.

- Momentum equation

$$\frac{\partial}{\partial x_j}\left(\rho \overline{u_i}\,\overline{u_j}\right) = -\frac{\partial p}{\partial x_i} + \frac{\partial}{\partial x_j}\left[\mu\left(\frac{\partial \overline{u_i}}{\partial x_j} + \frac{\partial \overline{u_j}}{\partial x_i}\right)\right] + \frac{\partial}{\partial x_j}\left(-\rho\overline{u_i' u_j'}\right), \tag{S2}$$

being p the pressure, μ the dynamic viscosity, and $\rho\overline{u_i' u_j'}$ the turbulent (or Reynolds) shear stress.

- Energy equation

$$\frac{\partial}{\partial x_i}(\rho \overline{u_i} T) = \frac{\partial}{\partial x_j}\left[\left(\frac{\mu}{\mathrm{Pr}} + \frac{\mu_t}{\mathrm{Pr}_t}\right)\frac{\partial T}{\partial x_j}\right], \tag{S3}$$

being T the temperature, Pr the Prandtl number and the subscript t referring to turbulent flow.

Considering the two-equation realizable $k-\varepsilon$ model with enhanced wall treatment:

$$\left(-\rho\overline{u_i'u_j'}\right) = \mu_t\left(\frac{\partial\overline{u}_i}{\partial x_j} + \frac{\partial\overline{u}_j}{\partial x_i}\right), \tag{S4}$$

where the dynamic turbulent viscosity is:

$$\mu_t = \rho C_\mu k^2/\varepsilon \tag{S5}$$

and the following transport equations hold for k and ε, respectively:

$$\frac{\partial}{\partial x_i}(\rho\overline{u}_i k) = \frac{\partial}{\partial x_j}\left[\left(\mu + \frac{\mu_t}{\sigma_k}\right)\frac{\partial k}{\partial x_j}\right] + \Gamma_k - \rho\varepsilon \tag{S6}$$

$$\frac{\partial}{\partial x_i}(\rho\overline{u}_i \varepsilon) = \frac{\partial}{\partial x_j}\left[\left(\mu + \frac{\mu_t}{\sigma_\varepsilon}\right)\frac{\partial \varepsilon}{\partial x_j}\right] + C_{\varepsilon 1}\frac{\varepsilon}{k}\Gamma_k + C_{\varepsilon 2}\rho\frac{\varepsilon^2}{k}. \tag{S7}$$

From Eq. (S5) to Eq. (S7), Γ_k and ε are respectively the turbulence kinetic energy generation and dissipation rates, $C_{\varepsilon 1} = 1.44$, $C_{\varepsilon 2} = 1.90$, $\sigma_k = 1.0$ and $\sigma_\varepsilon = 1.2$ are calibration parameters, while C_μ is computed by an eddy-viscosity equation (see further details in references [4, 5]).

ANSYS Fluent® was adopted for the numerical solution of the previous set of equations, considering the SIMPLE pressure-velocity coupling method. The "pseudo time steps" option was enabled and, after some trials, a Courant number varying between 1 and 2 revealed to be a good compromise to stabilize the iterative process for all the simulations. Besides the standard convergence conditions, the outlet temperature and heat exchanged through the inner tube surface have shown stable values for at least 20 consecutive iterations.

The "velocity-inlet" and "outflow" boundary conditions were considered for the air inlet and outlet, respectively (refer to the yellow frontiers in Fig. 3b). The inlet and outlet ports were designed as rectangular openings with the same length as the heat exchanger and a width equal to 30% of the fin diameter. The inlet air temperature was taken as 1000 K (therefore $\mu =$ 4.11 x 10^{-5} Pa·s and $\rho = 0.3627$ kg/m^3), while the Reynolds number was set to 600 in all the considered heat exchanger configurations and the inlet velocity calculated accordingly (the hydraulic diameter was computed as $D_h = \frac{2L_1L_2}{L_1+L_2}$, being L_1 and L_2 the sides of the rectangular inlets).

The Robin boundary condition was considered for the heat exchange through inner surface (refer to the green frontier in Fig. 3b). The free stream temperature of water $T_\infty =$ 293 K and the convective heat transfer coefficient $h \cong$ 5,000 W/m^2 K in the inner tube ($D_h = 15$ mm) were taken for all configurations. The latter has been estimated from the Dittus-Boelter correlation:

$$\mathrm{Nu} = 0.023\mathrm{Re}^{0.8}\mathrm{Pr}^{0.4}, \quad \text{(S8)}$$

being Nu the Nusselt number and considering the following water properties at T_∞: density $\rho = 1000$ kg/m^3, specific heat capacity $c_p = 4187$ J/kg K, thermal conductivity $\lambda = 0.6$ W/mK and kinematic viscosity $\nu = 5 \times 10^{-6}$ m^2/s. Considering a case study value of inlet water velocity of ≅2.5 m/s, Nu could be computed from Eq. (S8) and thus $h = \frac{\mathrm{Nu}\,\lambda}{D_h} \cong 5{,}000$ W/m^2 K obtained.

Finally, the homogeneous Neumann boundary condition (*i.e.*, null heat flux) was considered for the outer surface (refer to the orange frontier in Fig. 3b), to mimic a well-insulated external envelope of the heat exchanger.

SUPPLEMENTARY NOTE 2

To validate the numerical method adopted for the investigation, a comparison between the results obtained from CFD simulations and those estimated from well-established heat transfer correlations was carried out. Given the complexity of the finned configuration, a simpler heat exchanger without fins was considered for such comparison: the reference for this comparison was, therefore, the case of a plain tube hit by a perpendicular fluid cross-flow, whose heat transfer could be estimated by well-established correlations [6].

In this case, the characteristic length is defined as $L' = \frac{A}{U_{proj}}$, where A is the heat transfer surface and U_{proj} is the circumference of the active heat transfer area projected in the direction of the fluid flow. For a cylindrical tube, $L' = \frac{\pi\, d}{2}$ being d its external diameter. Then, $\mathrm{Nu}_{L'}$ was calculated as:

$$\mathrm{Nu}_{L'} = \mathrm{Nu}_{L',0} + \sqrt{\mathrm{Nu}^2_{L',lam} + \mathrm{Nu}^2_{L',turb}}\ , \quad \text{(S9)}$$

where $\mathrm{Nu}_{L',0}$ is the Nusselt number for static rounding, $\mathrm{Nu}_{L',lam}$ is the Nusselt number for the laminar flow surrounding area and $\mathrm{Nu}_{L',turb}$ is the Nusselt number for the turbulent regions, respectively calculated as:

$$\mathrm{Nu}_{L',0} = 0.3\ , \quad \text{(S10)}$$

$$\mathrm{Nu}_{L',lam} = 0.664\sqrt[3]{\mathrm{Pr}}\sqrt{\mathrm{Re}_{L'}}\ , \quad \text{(S11)}$$

$$\mathrm{Nu}_{L',turb} = \frac{0.037\ \mathrm{Re}^{0.8}_{L'}\ \mathrm{Pr}}{1 + 2.443\ \mathrm{Re}^{-0.1}_{L'}\ (\mathrm{Pr}^{2/3} - 1)} f_4\ , \quad \text{(S12)}$$

being f_4 a function that considers the influence of the direction of the heat flux defined as $f_4 = \left(\frac{T_{air}}{T_{tube}}\right)^{0.121}$. The heat transfer coefficient was then obtained as $h = \frac{\lambda\, Nu_{L'}}{L'}$, being λ the thermal conductivity of the air flowing over the tube. The total heat flux was finally calculated as:

$$Q = A\, h\, (T_{air} - T_{tube}), \tag{S13}$$

where the heat transfer surface A, that is the external surface of the inner tube, was calculated considering the total length of the heat exchanger, T_{air} was the same inlet air temperature considered in the simulations and T_{tube} was assumed to be the same as that of water flowing inside the inner tube. The Q estimated from the correlations from Eq. (S9) to Eq. (S13) was equal to 35.93 W, which compared to the 39.42 W obtained from the numerical model shown a discrepancy of 9.7%, that is coherent with the typical accuracy of convective heat transfer correlations.

SUPPLEMENTARY NOTE 3

In both Figs. 7 and 8, the chosen inlet air temperature was 1000 K. For the fluid dynamics conditions, rather than keeping the mass flow rate or the velocity constant, it has been chosen to lock the Reynold number (Re) and computing the corresponding air velocity. The reason is that the Nusselt number (Nu) and, ultimately, the convective heat transfer coefficient (h) both derive from Re rather than fluid velocity alone.

A case study value of Re=600 was then set in all configurations tested in Figs. 7 and 8. Considering a given inlet air temperature of 1000 K, the values of dynamic viscosity $\mu = 4.11 \times 10^{-5}$ Pa·s and density $\rho = 0.3627$ kg/m^3 were extracted from tables of properties for air. Then, the hydraulic diameter was calculated as

$$D_h = \frac{2L_1L_2}{L_1 + L_2}, \tag{S14}$$

being L_1 and L_2 the sides of the rectangular channel at the inlet. Finally, the inlet air velocity can be obtained as:

$$v = \frac{Re\, \mu}{\rho\, D_h}, \tag{S15}$$

with results reported in table below.

Fin size (D [mm] x tf [mm])	L_1 [mm]	L_2 [mm]	D_h [mm]	v [m/s]
40x0.5	13.5	12	12.7	5.35
60x0.5	13.5	18	15.4	4.41
80x0.5	13.5	24	17.3	3.49
40x1.5	16.5	12	13.9	4.89
60x1.5	16.5	18	17.2	3.95
80x1.5	16.5	24	19.6	3.48
40x3	21	12	15.3	4.45
60x3	21	18	19.4	3.51
80x3	21	24	22.4	3.04

SUPPLEMENTARY FIGURES

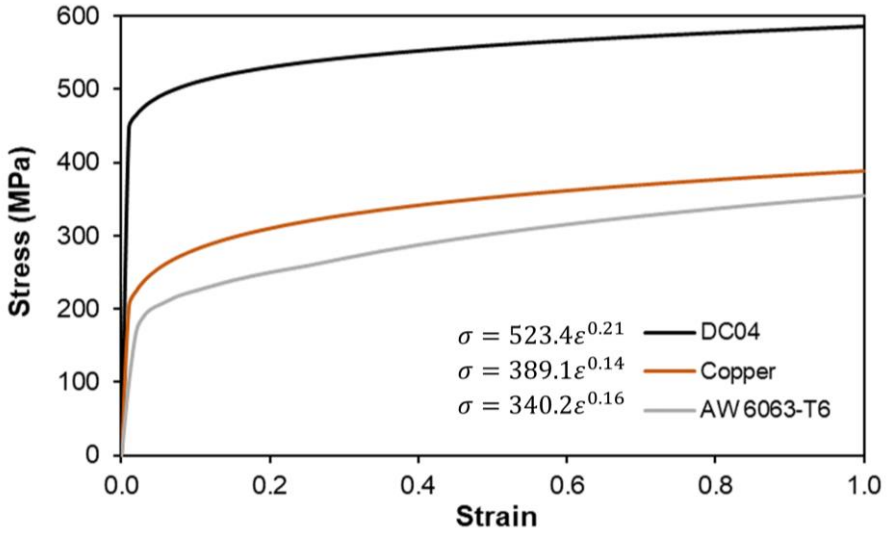

Supplementary Fig S1. Average material flow curves of aluminium AA6063-T6 tubes, copper sheets and steel DC04. Their respective power-law hardening equation (Ludwik-Holomon) is also included.

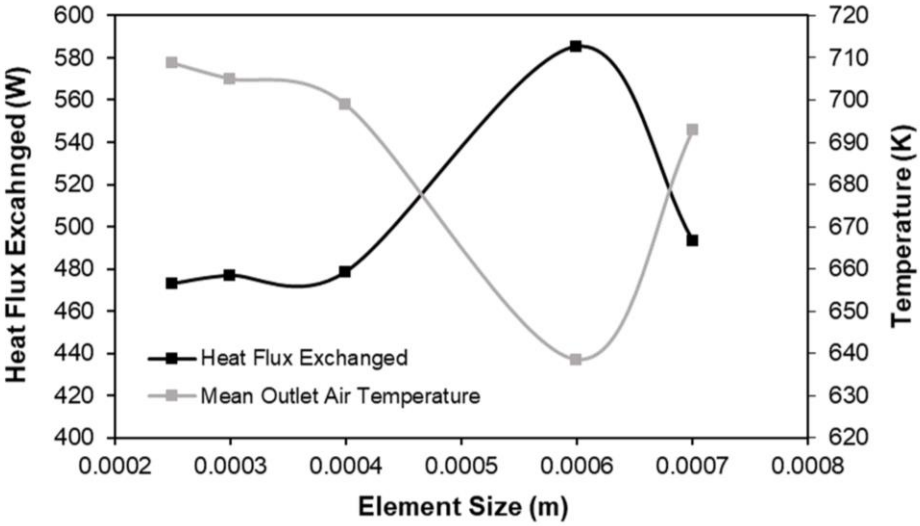

Supplementary Fig S2. Plot of heat flow rate exchanged and mean outlet air temperature for different element sizes to demonstrate mesh-independence of CFD simulations.

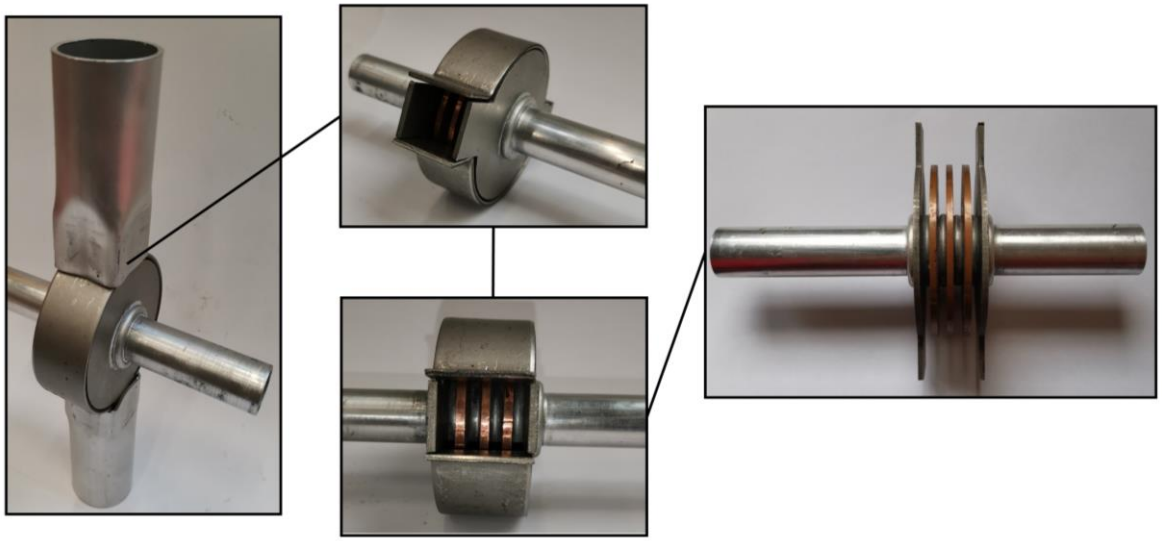

Supplementary Fig S3. Different views of the prototyped heat exchanger with details of the tube-fin mechanical connection system. The outer cases were removed during the characterization tests.

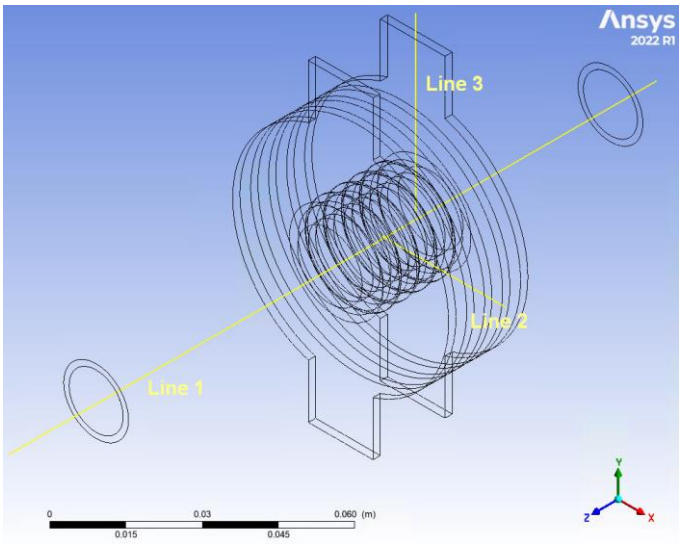

Supplementary Fig S4. Definition of the directions of interest for the analysis of the numerical temperature distribution.

SUPPLEMENTARY TABLE

Supplementary Tab S1. Temperature values measured at different points of Fig. 9 from experiments and simulations.

Measure point	Experimental (°C)	Numerical (°C)	Relative difference
P1	59.5	59.8	0.5%
P2	59.2	59.3	0.2%
P3	59.3	59.4	0.2%
Outlet water	59.9	59.9	0%

SUPPLEMENTARY REFERENCES

[1] E.P. Kumar, A.K. Solanki, M.M.J. Kumar, Numerical investigation of heat transfer and pressure drop characteristics in the micro-fin helically coiled tubes. Appl. Therm. Eng. 182 (2021), 116093. https://doi.org/10.1016/j.applthermaleng.2020.116093.

[2] C.D. Argyropoulos, N.C. Markatos, Recent advances on the numerical modelling of turbulent flows. Appl. Math. Model. 39 (2015), 693-732. https://doi.org/10.1016/j.apm.2014.07.001.

[3] ANSYS FLUENT 2021 R2, Theory Guide (2021).

[4] T.-H. Shih, W.W. Liou, A. Shabbir, Z. Yang, J. Zhu, A new k-ϵ eddy viscosity model for high Reynolds number turbulent flows. Computers & Fluids. 24 (1995), 227-238. https://doi.org/10.1016/0045-7930(94)00032-T.

[5] R. Şibil, E. Aras, M. Kankal, Comparison of various turbulence model performance in computational fluid dynamics analyses of the oxidation ditches with experimental validation. Process Saf. Environ. Prot. 154 (2021), 43-59. https://doi.org/10.1016/j.psep.2021.07.046.

[6] P. Böckh, T. Wetzel, Heat transfer: basics and practice, Springer, London, 2012. https://doi.org/10.1007/978-3-642-19183-1.